Title

Superior Efficacy and Selectivity of Novel Small-Molecule Kinase Inhibitors of T790M-Mutant EGFR in Preclinical Models of Lung Cancer

Journal

Cancer Research, 77(5)

ISSN

0008-5472

Authors

Rho, Jin Kyung
Lee, In Yong
Choi, Yun Jung
et al.

Publication Date

2017-03-01

DOI

10.1158/0008-5472.can-16-2432

Peer reviewed

Published in final edited form as:

Cancer Res. 2017 March 01; 77(5): 1200–1211. doi:10.1158/0008-5472.CAN-16-2432.

Superior efficacy and selectivity of novel small molecule kinase inhibitors of T790M mutant EGFR in preclinical models of lung cancer

Jin Kyung Rho[1,2,3,*], **In Yong Lee**[4], **Yun Jung Choi**[1,3], **Chang-Min Choi**[3,5], **Jae-Young Hur**[1,3], **Jong Sung Koh**[4], **Jaekyoo Lee**[4], **Byung-Chul Suh**[4], **Ho-Juhn Song**[4], **Paresh Salgaonkar**[4], **Jungmi Lee**[4], **Jaesang Lee**[6], **Dong Sik Jung**[6], **Sang-Yeob Kim**[1,2], **Dong-Cheol Woo**[1,2], **In-Jeoung Baek**[1,2], **Joo-Yong Lee**[1,2], **Chang Hoon Ha**[1,2], **Young Hoon Sung**[1,2], **Jeong Kon Kim**[7], **Woo Sung Kim**[3], **Joon Seon Song**[8], **Cheol Hyeon Kim**[9], **Trever G. Bivona**[10,11,*], and **Jae Cheol Lee**[5,*]

[1]Asan Institute for Life Sciences, Asan Medical Center, College of Medicine, University of Ulsan, Seoul. Korea

[2]Department of Convergence Medicine, Asan Medical Center, College of Medicine, University of Ulsan, Seoul. Korea

[3]Department of Pulmonology and Critical Care Medicine, Asan Medical Center, College of Medicine, University of Ulsan, Seoul, Korea

[4]Genosco, Massachusetts, MA, USA

[5]Department of Oncology, Asan Medical Center, College of Medicine, University of Ulsan, Seoul, Korea

[6]Oscotec Inc., Seongnam, Korea

[7]Department of Radiology, Research Institute of Radiology, Asan Medical Center, College of Medicine, University of Ulsan, Seoul, Korea

[8]Department of Pathology, Asan Medical Center, College of Medicine, University of Ulsan

[9]Department of Internal Medicine, Korea Cancer Center Hospital, Seoul, Korea

[10]Department of Medicine, University of California San Francisco, San Francisco, CA

[11]Helen Diller Family Comprehensive Cancer Center, University of California San Francisco, San Francisco, CA

Abstract

[*]Co-corresponding authors: Jin Kyung Rho Ph.D. (jkrho@amc.seoul.kr), Trever G. Bivona M.D. Ph.D. (Trever.Bivona@ucsf.edu) or Jae Cheol Lee M.D. Ph.D. (jclee@amc.seoul.kr).
J. K. Rho and I. Y. Lee contributed equally to this work.

Potential Conflict of Interest. In Yong Lee, Jong Sung Koh, Jaekyoo Lee, Byung-Chul Suh, Ho-Juhn Song, Paresh Salgaonkar, Jungmi Lee are employees of Genosco, MA, USA, which developed the GNS compounds reported in this study. The other authors declare no conflicts of interest.

The clinical utility of approved EGFR small molecule kinase inhibitors is plagued both by toxicity against wild-type EGFR and by metastatic progression in the central nervous system (CNS), a disease sanctuary site. Here we report the discovery and preclinical efficacy of GNS-1486 and GNS-1481, two novel small molecule EGFR kinase inhibitors that are selective for T790M mutant isoforms of EGFR. Both agents were effective in multiple mouse xenograft models of human lung adenocarcinoma (T790M positive or negative), exhibiting less activity against wild-type EGFR than existing approved EGFR kinase inhibitors (including osimertinib). Additionally, GNS-1486 showed superior potency against intracranial metastasis of EGFR-mutant lung adenocarcinoma. Our results offer a preclinical proof of concept for new EGFR kinase inhibitors with the potential to improve therapeutic index and efficacy against brain metastases in patients.

Introduction

Lung cancer is the leading cause of cancer mortality worldwide, with lung adenocarcinoma (LA) as the most common histologic subtype (1) (2). The clinical success of oncogene-targeted therapy in specific subsets of LA patients, such as those with activating mutations in EGFR, has heralded a new era of precision cancer medicine with great promise for improving patient survival and quality of life (3) (4–10). However in the case of EGFR-mutant LA, both clinical toxicity due to residual activity against WT EGFR versus mutant EGFR and metastatic tumor progression in the CNS are two remaining obstacles that limit the overall clinical impact of the current first-(gefitinib, erlotinib), second-(afatinib), and third-generation (osimertinib) EGFR TKIs that are FDA-approved (11) (12) (13–18) (19). Importantly, LA patients with CNS metastasis have a particularly dismal prognosis, as no drug therapy has shown consistent or durable efficacy against intracranial metastasis to date (19, 20).

During the treatment of EGFR-mutant LA patients with first-generation EGFR TKIs (erlotinib, gefitinib), tumor progression often occurs via the emergence of the $EGFR^{T790M}$ resistance mutation (21, 22). This observation prompted the development of second- and third-generation irreversible EGFR inhibitors with activity against $EGFR^{T790M}$ (21, 23, 24). Some of these newer EGFR inhibitors such as CO-1686 (rociletinib) and AZD9291 (osimertinib) exhibit increased selectivity for mutant EGFR with relative sparing of WT EGFR, as compared to earlier EGFR inhibitors including erlotinib, gefitinib, and afatinib (12). This relative selectivity for mutant EGFR over WT EGFR can enhance the therapeutic index for EGFR inhibition in patients, potentially reducing certain toxicities that occur because of WT EGFR blockade (such as cutaneous and gastrointestinal side effects) (25, 26). While the development of CO-1686 (Rociletinib) has been discontinued (in part due to less impressive clinical efficacy than initially anticipated), AZD9291 (osimertinib) is now approved for the second-line treatment of LA patients with $EGFR^{T790M}$-positive disease (25, 26). Although osimertinib appears to be associated with decreased clinical toxicity (by historical comparison to first- and second-generation EGFR TKIs), side effects linked to residual activity against WT EGFR remain a clinical challenge and impair the quality of life in patients (including grade 3 adverse events occurring in ~33% of osimertinib-treated individuals) (25–28) (toxicity that is consistent with the experience using osimertinib in our own clinical practices). In addition to the clinical toxicity and quality of life issues, the

recommended drug dose (or in some cases dose reduction or suspension) that is used as a consequence of the toxicity resulting from the sub-maximal selectivity for mutant EGFR over WT EGFR of the current FDA-approved EGFR TKIs can lead to incomplete (or non-sustained) target inhibition in both intracranial and extracranial tumor cells, thereby potentially contributing to the progression of metastatic tumors both within and outside of the CNS (11) (21, 26, 29).

Disease progression in the CNS, a sanctuary site, is a widespread cause of death in EGFR-mutant LA patients (19). Limited published reports show that the current approved EGFR inhibitors (including osimertinib) have documented but inconsistent and often temporary clinical efficacy against CNS metastases (7) (19) (24) (25, 26, 30) (31) (abstracts: Kim D et al. Annals of Oncology (2014) 25 (suppl_4): iv146-iv164. 10.1093/annonc/mdu331; Camidge DR et al. MINI16.04, 16th World Conference on Lung Cancer, 2015; Sequist LV et al. J Clin Oncol. 2014;32(15 Suppl):abstract 8010). There remains no established and widely effective systemic treatment for CNS metastases in patients with EGFR-mutant LA; and progression of CNS metastasis has been reported and observed in our own clinical practices in patients treated with all current FDA-approved EGFR inhibitors, including osimertinib (19, 28, 32) (Ahn MJ, et al. ESMO 2015. Abstract 3083). Thus, although recently initiated clinical trials are testing certain EGFR TKIs such as osimertinib in patients with CNS metastasis (e.g. NCT02736513), the CNS anti-tumor efficacy of the EGFR TKIs that are currently approved remains an unresolved and active area of investigation.

To address the limitations of the current approved EGFR TKIs, we conducted a drug discovery program to discover a potent, mutant-selective EGFR TKI with less WT EGFR activity and thus potentially a wider therapeutic index versus the currently approved EGFR TKIs and that also exhibits pronounced activity against intracranial EGFR-mutant LA metastasis. This discovery program has led to the identification of two novel and improved EGFR TKIs; the data provide the rationale for clinical trials that will be initiated soon testing these promising new agents in EGFR-mutant (including EGFR^{T790M}) LA patients with intracranial and extracranial metastatic disease.

Materials and Methods

Cell Culture and Reagents

The human NSCLC cell lines (HCC827 and H1975) and NIH 3T3 (mouse embryonic fibroblast cell line) were obtained from the American Type Culture Collection (Rockville, MD). PC-9 cells were a gift from F. Koizumi and K. Nishio (National Cancer Center Hospital, Tokyo, Japan). PC-9/GR (gefitinib-resistant cell line) and PC-9/ER (erlotinib-resistant cell line) cells were established as part of a previous study (33). Cells were cultured in RPMI 1640 medium containing 10% FBS, 2 mmol/L L-glutamine, and 100 units/mL of penicillin and streptomycin, and maintained at 37 °C in a humidified chamber containing 5% CO_2. Osimertinib, CO-1686 and WZ4002 were purchased from Selleck Chemicals (Houston, TX). The cell lines used were authenticated by STR analysis and confirmed to be mycoplasma free using standard methods.

Cellular Viability Assays

To perform the MTT assay, cells (5×10^3) were seeded in 96-well sterile plastic plates for overnight and then treated with relevant agents. After 72 h, 15 μL of MTT solution (5 mg/mL) was added to each well and plates were incubated for 4 h. Crystalline formazan was solubilized with 100 μL of a 10% (w/v) SDS solution for 24 h, and then absorbance at 595 nm was read spectrophotometrically using a microplate reader. To test the colony formation assay, cells ($0.1–1 \times 10^3$) were seeded in 6-well plates and then treated with relevant agents. After 10–14 days, the colonies were stained with crystal violet and counted. The results are representative of at least three, independent experiments, and the error bars signify standard deviations (SDs).

Cell-free Kinase Assay

Cell-free kinase assays were conducted using Lance Ultra time-resolved fluorescence resonance energy transfer (TR-FRET) technology according to the manufacturer's instructions (Perkin-Elmer). Briefly, various concentrations of EGFR inhibitors were mixed with each enzyme (wildtype or mutant EGFR, Her2, and Her4), the Ulight-poly-GT peptide substrate and ATP in a kinase buffer (50 mM HEPES pH 7.5, 10 mM MgCl2, 1mM EFTA, 2 mM DTT and 0.01% Tween-20) in a 96 well plate. Kinase reactions were incubated at room temperature for 1 hour and then stopped by addition of EDTA. The specific Europium-labeled anti-phosphopetide antibody (Perkin-Elmer) was added to the reaction in Lance detection buffer. The mixture was allowed to incubate for 30 minute to allow binding of the antibody to the phosphorylated site before the plate was read. The LANCE signal was measured on an EnVision Multilabel Reader (Perkin Elmer). Excitation wavelength was set at 320 nm and emission was monitored at 615 nm (doner) and 665 nm (acceptor). The IC_{50} values were determined using GraphPad prism software.

Kinase Profile Assay

The kinase selectivity was assessed by KinaseProfiler (Millipore, UK) consisting of 321 kinases for GNS-1481 or 323 kinases for GNS-1486 and osimertinib at a single concentration of 1 μM using ATP Km for each kinase.

Expression Vectors and Transfections

EGFR constructs (EGFR wild-type, EGFR del746-750, EGFR T790M/L858R, and EGFR T790M/del746-750) were purchased from Addgene (Cambridge, MA). Transfections were performed using Lipofectamine 2000 (Invitrogen) in accordance with the manufacturer's instructions. Transfected cells were selected using puromycin (2 μg/mL for NIH3T3; Sigma).

Immunoblotting

Cells were lysed in buffer containing 137 mmol/L NaCl, 15 mmol/L EGTA, 0.1 mmol/L sodium orthovanadate, 15 mmol/L $MgCl_2$, 0.1% Triton X-100, 25 mmol/L MOPS, 100 mmol/L phenylmethylsulfonyl fluoride, and 20 mmol/L leupeptin, adjusted to pH 7.2. Lysis of tumor specimens was performed using Omni Tissue Homogenizer (TH; Omni International, Kennesaw, GA). Antibodies specific for p-EGFR (Tyr1173), EGFR, Akt,

ERK, and actin were obtained from Santa Cruz Biotechnology (Santa Cruz, CA), and antibodies for PARP, caspase 3, p-Akt (Ser473) and p-ERK (Thr202/Tyr204) were purchased from Cell Signaling Technology (Beverly, MA). Proteins were detected with an enhanced chemiluminescence Western blotting kit (Amersham Biosciences), according to the manufacturer's instructions.

Animal Models

To establish xenograft model, female severe combined immunodeficiency (SCID) mice (18–20 g, 6 weeks of age) were purchase from Charles River Laboratories. All experimental procedures were conducted following a protocol approved by the Institutional Animal Care and Use committee of Asan Institute for Life Sciences (2014-12-103 and 2015-12-087). Tumors were grown by implanting cells ($1–5 \times 10^6$ cells/0.1 mL) in 50% Matrigel (BD Biosciences) and subcutaneously injected into the right flank of animals. Drug treatment was started when the tumors reached a volume of 50–100 mm^3. To measure tumor size, the length (L) and width (W) of each tumor was measured using calipers, and tumor volume (TV) was calculated as $TV = (L \times W^2)/2$. To perform the intracranial implantation of HCC827-luc cells, the human NSCLC cell line HCC827 was stably integrated with a luciferase reporter gene, RediFect lentiviral particles (PerkinElmer). Female athymic nude mice (6–8 weeks of age, Charles River Laboratories) were anesthetized with a ketamine/xylazine cocktail solution. The head of the mouse was stabilized by using a Harvard Apparatus stereotaxic head frame. After disinfection of the skin, a 1 cm midline scalp incision was made, and a burr hole (coordinates: 2.5 mm lateral and 0.5 mm posterior to the bregma) in the skull was made by using a high-speed micro-drill. Cells ($1–5 \times 10^5$ cells/4 μL serum-free RPMI) were injected into the right striatum using a 10 μL Hamilton syringe to deliver tumor cells to a 3.5-mm intraparenchymal depth. The burr hole in the skull was sealed with bone wax and the incision closed using Dermabond. Tumor growth was monitored and measured via bioluminescence imaging in vivo.

Drug Administration

GNS-1481 and 1486 dissolved in NMP/PEG300 (1:9, v/v), and osimertinib and CO-1686 dissolved in Tween-80. All drugs were given by oral intubation for the indicated times.

Bioluminescence Monitoring and μCT Co-registration of Intracranial Tumors

Intracranial tumor growth was quantified by bioluminescence imaging (BLI) was performed using an IVIS spectrum system (Caliper, Perkinelmer company, Alameda, California). Mice were administered by intraperitoneal injection with 150mg/kg body weight of D-Luciferin (Caliper Life Science, Hopkinton, MA) dissolved in DPBS (Gibco). Before and during imaging, mice were anesthetized by 1% isoflurane inhalation (Forane®, Choongwae, Korea). Bioluminescent signals were acquired with open filter or emission at 620nm using auto acquisition and field of view of 13.4 cm, and bioluminescent signals were quantified as radiance (photon/sec/cm^2/sr) within a circular region of interest (ROI) using Living Image® 4.4 software. To visualize the anatomical location, mice were imaged with a Quantum FX μCT system after optical imaging. μCT image used a 120mm FOV with a 236μm voxel size and dose of 26mGy per scan. 3-dimensional optical and reconstructed μCT images were

automatically generated with the Living Image® 4.4 Software and 3D ROIs were measured as voxels (photons/sec).

Immunohistochemical Staining (IHC)

Each tumor was harvested the indicated times post administration with drugs. Resected tumors were fixed in 10% formaldehyde and embedded in paraffin. Immunohistochemical staining was done using specific primary antibody (Ki-67; DakoCytomation, Los Angeles, CA), the EnVision Plus staining kit (DakoCytomation) and APO-Direct terminal deoxynucleotidyl transferase–mediated dUTP nick end labeling (TUNEL) assay kit (Millipore) according to the supplier's instructions. Quantitative analysis of section staining was done by counting immunopositive cells in 5 arbitrarily selected fields.

Statistical analysis

P values were determined with unpaired t-tests between comparator groups using Graphpad software.

Results

Discovery and characterization of novel mutant-selective EGFR TKIs

In search of novel wild type (WT) or mutant EGFR (Del 19, E746-A750), L858R, L858R/T790M, T790M, Del 19/T790M) inhibitors, we performed a high-throughput screen (HTS) of a proprietary compound library consisting of 1583 structurally-diverse molecules. This campaign led to the identification of 30 compounds displaying activity against mutant EGFR. Structure-based drug design utilizing structure activity relationship (SAR) information from the 30 hit compounds led to several potent and selective inhibitors with favorable physical properties and *in vitro* ADME (absorption, distribution, metabolism and excretion). Among those 30 compounds, two novel 3-pyrazolypyrimidine compounds (GNS-1481 and GNS-1486) were identified as potent and selective irreversible EGFR inhibitors against all forms of mutant EGFR tested. GNS-1481 and GNS-1486 contain a pyrimidine-based scaffold, analogous to other third-generation EGFR kinase inhibitors (23, 24) (Figure 1A–B). GNS-1481 and GNS-1486 exhibited broad activity at low nanomolar concentrations against all EGFR mutations tested, including $EGFR^{T790M}$ in kinase inhibition *in vitro* assays (Table 1). Moreover, GNS-1481 and GNS-1486 showed substantial selectivity for mutant EGFR as compared to WT EGFR, as indicated by the selectivity index (defined as the ratio of the IC_{50} for WT EGFR/IC_{50} for the L858R-T790M double mutant, Table 1, bottom row). GNS-1486, in particular, showed superior selectivity for mutant EGFR over WT EGFR compared to the other approved EGFR inhibitors, including osimertinib (Table 1). Structural modeling studies of the thermodynamics and binding of GNS-1481 and GNS1486 to either WT or mutant EGFR suggested distinct interactions enabling a tighter association with mutant EGFR versus WT EGFR overall and improved mutant selectivity compared to osimertinib in general, consistent with the kinase profiling studies (Figure S1, Table 1). These findings indicating the substantial potency and mutant EGFR selectivity of the GNS compounds were further extended across a panel of ~320 kinases in a multi-kinase inhibition assay *in vitro* (Figure 1C, Table S1). While strong activity against various forms of mutant EGFR was observed for GNS-1481 and GNS-1486 (each tested at 1 μM), these

agents exhibited less or minimal activity against WT EGFR or other EGFR family members such as ErbB2 and ErbB4 when compared to osimertinib (Figure 1C, Table S1). Interestingly, we noted that GNS-1481 and GNS-1486, in contrast to osimertinib, exhibited *in vitro* activity against RET (either WT or the gatekeeper mutant V804L that is resistant to certain other RET inhibitors (34)), an oncogene in other tumor types including thyroid cancer and a distinct subset of LA driven by RET gene rearrangements (34) (35) (Figure 1C, Table S1). Furthermore, GNS-1481 and GNS-1486 showed unique activity against MLK1 (mixed-lineage kinase 1), which can activate MEK-ERK signaling and promote RAF inhibitor resistance in melanoma (36) (Figure 1C, Table S1). Together, these biochemical data reveal the high potency, substantial mutant EGFR selectivity, and unique target profiles of the two novel irreversible EGFR inhibitors we identified, GNS-1481 and GNS-1486.

Preclinical efficacy of the novel mutant-selective EGFR kinase inhibitors GNS-1481 and GNS-1486 *in vitro*

We next examined the activity of both GNS-1481 and GNS-1486 on signaling and cell viability in EGFR-mutant preclinical models. We first studied the impact of treatment with each agent and with other third-generation EGFR inhibitors (osimertinib, CO-1686, WZ4002) (37) on signaling in NIH-3T3 cells engineered to express either WT or mutant EGFR (Del 19, Del 19/T790M, L858R/T790M) (Figure 2A–B). GNS-1481 and GNS-1486 had comparatively minimal impact on the levels of phosphorylated (p)-EGFR, or the downstream signaling components p-ERK and p-AKT, in WT EGFR-expressing cells, consistent with the WT EGFR-sparing activity of these agents observed in the biochemical assays (Figure 2B, S2A). In contrast, treatment with each agent suppressed the levels of p-EGFR, p-ERK, and p-AKT and induced cleavage of PARP (as a measure of apoptosis) in each EGFR-mutant model (Figure 2A–B, S2A–B). We did not find substantial *in vitro* activity of the GNS agents against the C797S mutant form of EGFR that can promote resistance to other third-generation EGFR inhibitors such as osimertinib (data not shown) (27).

We next assessed the effects of GNS-1481 and GNS-1486 treatment on cell viability in human EGFR-mutant LA cell lines, including those with $EGFR^{T790M}$. We found that treatment with either agent was highly effective against multiple EGFR-mutant models *in vitro* (including PC9 and HCC827 cells with Del 19) (Figure 3A–B, Table S2). Moreover, GNS-1481 and GNS-1486 exhibited substantial efficacy in $EGFR^{T790M}$-positive LA models *in vitro*, including PC-9/GR and PC-9/ER sub-lines with acquired resistance to gefitinib or erlotinib (33, 38), respectively, and H1975 cells that intrinsically harbor $EGFR^{L858R/T790M}$ (Figure 3A–B, Table S2). We further established the specificity of GNS-1481 and GNS-1486 efficacy for lung cancer cells with mutant EGFR by testing these agents in multiple EGFR WT lung cancer models, including A549, H460, and A341 cells. We found no significant impact of treatment with either agent on cell viability in these models (Figure S2C). GNS-1481 and GNS-1486 (or osimertinib) monotherapy had no significant effect on the viability of EGFR-mutant LA cells with acquired erlotinib/gefitinib resistance driven by non-$EGFR^{T790M}$-mediated mechanisms such as MET and AXL kinase upregulation, as expected (Figure S2D) (39, 40). Together, these findings further establish the substantial and

specific activity of GNS-1481 and GNS-1486 in multiple $EGFR^{T790M}$ (-) and (+) EGFR-mutant LA preclinical models.

Analysis of the impact of GNS-1481 and GNS-1486 treatment on key signaling components in the EGFR-mutant LA models (PC-9, PC-9/GR, PC-9/ER, H1975) revealed that each agent suppressed the levels of p-EGFR, p-ERK, and p-AKT in each system (Figure 3C, S2E). Treatment with GNS-1481 and GNS-1486 was lethal in these EGFR-mutant LA cell lines, as these effects on signaling were accompanied by the induction of apoptosis upon GNS-1481 and GNS-1486 treatment, indicated by increased levels of both cleaved PARP and Caspase-3 (Figure S2F). Together, these data indicate that GNS-1481 and GNS-1486 are novel mutant-selective EGFR inhibitors that strongly suppress mutant EGFR signaling and induce apoptosis, resulting in substantial efficacy in multiple $EGFR^{T790M}$ (−) and (+) EGFR-mutant LA preclinical models. Overall, we noted in these *in vitro* studies that the GNS agents showed superior WT EGFR-sparing properties compared to the other clinically approved EGFR TKIs and demonstrated therapeutic effects that are comparable to the other third-generation EGFR inhibitors tested (with relatively subtle differences observed across these *in vitro* systems and the parameters measured).

Preclinical efficacy of the novel mutant-selective EGFR kinase inhibitors GNS-1481 and GNS-1486 *in vivo*

Supported by our encouraging findings showing improved sparing of WT EGFR, substantial mutant EGFR-selective potency, and efficacy *in vitro*, we next investigated the *in vivo* properties of GNS-1481 and GNS-1486, including pharmacokinetic (PK), pharmacodynamic (PD), safety, and anti-tumor efficacy analysis. *In vivo* pharmacology and PK studies in mouse, rat, and dog revealed substantial exposure upon oral administration at 10 mg/kg for mouse and rat and 5 mg/kg for dog (Figure S3A, data not shown). This oral dosing regimen achieved plasma concentrations near or above 1 μM (particularly in mouse and dog) (Figure S3A, data not shown). Furthermore, this PK analysis demonstrated a half-life predictive of once-daily oral dosing for each agent (or potentially twice-daily for GNS-1481 pending ongoing *in vivo* PK assessment) (Figure S3A, data not shown). Importantly, no systemic toxicity was noted in the animals during the PK and dose-finding studies (data not shown).

We further tested the efficacy of GNS-1481 and GNS-1486 treatment against multiple human EGFR-mutant LA models implanted subcutaneously into mice, including models with $EGFR^{T790M}$ (PC-9/GR and H1975) (Figure 4A). We found that once-daily oral treatment with either agent demonstrated substantial *in vivo* efficacy in each model, inducing sustained tumor regressions in PC-9 and PC-9/GR tumors and initial regressions and subsequent disease control in H1975 tumors (Figure 4A). The efficacy of GNS-1481 and GNS-1486 was similar to gefitinib in the PC9 ($EGFR^{Del\ 19}$) tumor xenografts, and superior to gefitinib in the PC9/GR ($EGFR^{Del19/T790M}$) and H1975 ($EGFR^{L858R/T790M}$) tumor xenografts, as expected given that gefitinib is largely inactive against $EGFR^{T790M}$-positive cancers (Figure 4A). The anti-tumor efficacy of GNS-1481 and GNS-1486 occurred without substantial overt toxicity in the treated animals (Figure S3B, data not shown). Analysis of key PD biomarkers including p-EGFR, p-AKT, and p-ERK indicated that GNS-1481 and

GNS-1486 substantially suppressed EGFR activation and downstream signaling (Figure 4B–C). These effects of GNS-1481 and GNS-1486 treatment on signaling were accompanied by decreased proliferation (as measured by quantitative analysis of Ki-67 staining in the tumor cells by immunohistochemistry) and increased apoptosis (as measured by quantitative analysis of TUNEL staining in the tumor cells by immunohistochemistry) (Figure 4D–E). Moreover, we compared the activity of the GNS agents to osimertinib in two distinct $EGFR^{T790M}$-positive *in vivo* models and, overall, found comparable anti-tumor and signaling effects in response to treatment with each drug (Figure S4A–D). However, we found that both GNS-1486 and GNS-1481 showed less activity against WT EGFR in the skin of treated animals in multiple different *in vivo* systems, compared to treatment with either erlotinib or osimertinib and at doses where p-EGFR inhibition in the tumors (H1975) *in vivo* was equivalent between the GNS agents and osimertinib (Figure S4E–F). Together, these data indicate that GNS-1481 and GNS-1486 show substantial mutant EGFR-selective, oral anti-tumor efficacy with less activity against WT EGFR *in vivo* than currently approved EGFR TKIs (including osimertinib), offering a potentially wider safety margin than these current EGFR TKIs while showing substantial anti-tumor efficacy.

Intracranial anti-tumor efficacy of the novel mutant-selective EGFR kinase inhibitor GNS-1486 *in vivo*

During the preclinical pharmacology and PK *in vivo* analysis, we noted that GNS-1481 and GNS-1486 exhibited substantial CNS penetration, with intravenous (IV) administration in rats resulting in a CNS/plasma concentration ratio of 0.53–6.15 within two hours of initial dosing (Table S3). These observations suggested that GNS-1481 or GNS-1486 could potentially show efficacy against intracranial tumors *in vivo*. We tested this hypothesis by establishing intracranial tumors in mice using human EGFR-mutant (Del 19) LA cells engineered to stably express a luciferase reporter to enable *in vivo* bioluminescence-based monitoring of tumor growth (HCC827-Luc cells, Figure 5A). Intracranial implantation of HCC827-Luc cells resulted in substantial tumor growth in the brain within 2–3 weeks, confirmed by both bioluminescence imaging and by pathologic analysis of brain sections obtained from tumor-bearing mice (Figure 5A–B). We then treated mice with established intracranial EGFR-mutant LA with once-daily orally administered GNS-1486 and assessed CNS tumor growth *in vivo*, making comparison to osimertinib as the only approved third-generation EGFR inhibitor and which has shown some CNS activity in limited published reports (30) (31). Importantly, the CNS activity of osimertinib and other EGFR TKIs in patients remains under active clinical investigation and has not yet been firmly established in large patient cohorts (to our knowledge). GNS-1486 was chosen for study because of its better selectivity for mutant EGFR over WT EGFR, and its improved PK parameters compared to GNS-1481. We found that once-daily oral GNS-1486 substantially suppressed intracranial tumor growth in these mice, as measured both by bioluminescence imaging and micro-CT (computerized tomography) (Figure 5C–G). In an animal with a large detectable spinal metastasis, we further noted excellent *in vivo* activity of GNS-1486 against both the primary brain and spinal tumors, consistent with the substantial CNS penetration demonstrated by this agent (Figure S5A). We found that CO-1686 (rociletinib) did not, but osimertinib did show CNS activity in the HCC827 intracranial tumor system (Figure 6A–D, data not shown), consistent with prior data (30). However, GNS-1486 showed increased

potency versus osimertinib against the CNS metastases in this *in vivo* system, as evidenced by the increased efficacy of GNS-1486 versus osimertinib at the 3mg/kg/day dosing of each agent (measured by quantitative BLI analysis and comparison; P=0.044 for 3mg/kg GNS-1486 superiority versus 3mg/kg osimertinib at 1 week and P=0.007 for 3mg/kg GNS-1486 superiority versus 3mg/kg osimertinib at 2 weeks) (Figures 5D–F, 6B–E).

Consistent with these observations, we found that GNS-1486 treatment suppressed p-EGFR, p-AKT, and p-ERK levels and increased apoptosis as measured by both cleaved PARP and Caspase3 levels in the intracranial tumors, again with an improved potency compared to osimertinib as shown by the increased efficacy of GNS-1486 versus osimertinib in the 3mg/kg/day treatment cohorts (p-EGFR: P<0.0001 for 3mg/kg GNS-1486 superiority versus 3mg/kg osimertinib; p-Akt: P=0.004 for 3mg/kg GNS-1486 superiority versus 3mg/kg osimertinib; p-Erk: P=0.015 for 3mg/kg GNS-1486 superiority versus 3mg/kg osimertinib; cleaved PARP: P=0.028 for 3mg/kg GNS-1486 superiority versus 3mg/kg osimertinib; cleaved caspase3: P=0.018 for 3mg/kg GNS-1486 superiority versus 3mg/kg osimertinib (Figure S5B). Superior *in vivo* pharmacodynamics of GNS-1486 versus osimertinib were also observed at the higher 10 mg/kg/day cohorts for certain PD biomarkers (p-Erk: P=0.049 for 10mg/kg GNS-1486 superiority versus 10mg/kg osimertinib; cleaved PARP: P=0.016 for 10mg/kg GNS-1486 superiority versus 10mg/kg osimertinib; cleaved caspase3: P=0.024 for 10mg/kg GNS-1486 superiority versus 10mg/kg osimertinib; p-EGFR: P=0.16 for 10mg/kg GNS-1486 versus 10mg/kg osimertinib; p-Akt: P=0.334 for 10mg/kg GNS-1486 versus 10mg/kg osimertinib); in contrast to the 3mg/kg/day comparison between GNS-1486 and osimertinib, these improved PD effects at the 10 mg/kg dose were not associated with statistically significant differences in the anti-tumor efficacy as measured by BLI analysis at these higher drug doses and time points in this system (P=0.28 for 10mg/kg GNS-1486 versus 10mg/kg osimertinib at 1 week; P=0.9 for 10mg/kg GNS-1486 versus 10mg/kg osimertinib at 2 weeks) (Figures 5D–F, 6B–D).

We further found that treatment with GNS-1486 substantially improved survival in mice with intracranial EGFR-mutant tumors (using the HCC827-Luc system) (Figure 6E). We again noted an improved potency of GNS-1486 compared to osimertinib in these preclinical trials, as evidenced by the efficacy outcome data in the 3mg/kg/day treatment cohorts (P=0.0035 for 3mg/kg GNS-1486 superiority versus 3mg/kg osimertinib; P=0.7519 for 10mg/kg GNS-1486 versus 10mg/kg osimertinib). We further confirmed the substantial intracranial anti-tumor activity of GNS-1486 in an additional patient-derived EGFR-mutant LA model (H1975 $EGFR^{L858R/T790M}$ cells) (Figure S6). In contrast, CO-1686 (rociletinib) treatment was less effective in this intracranial H1975 tumor system (Figure S6). Importantly, no signs of systemic or CNS toxicity were noted during treatment with GNS-1486 in the mice (data not shown), consistent with the high selectivity for mutant EGFR versus WT EGFR we observed for this agent. The data suggest that GNS-1486 exhibits superior potency against EGFR-mutant LA CNS disease versus osimertinib (and rociletinib) in these *in vivo* systems, offering a new highly effective therapeutic agent whose potency and selectivity for mutant EGFR provides the potential advantage of decreased clinical toxicity. Altogether, these findings establish GNS-1486 as a novel, improved, orally administered, CNS-penetrant, and mutant-selective EGFR (including $EGFR^{T790M}$) inhibitor with both potent extracranial and intracranial anti-tumor efficacy and a wide apparent safety

margin. The data provide the rationale for clinical trials testing the safety and efficacy of GNS-1486 in EGFR-mutant (including $EGFR^{T790M}$) LA patients with active CNS metastatic disease (as well as extracranial disease); these trials will be initiated soon.

Discussion

In summary, despite recent important progress in the field, the identification of a potent, more mutant EGFR-selective and CNS-active EGFR TKI with an improved safety margin could have a substantial and immediate beneficial impact on both patient outcomes and quality of life. Towards this end, our study establishes the preclinical efficacy, safety, and potential clinical utility of novel mutant-selective EGFR TKIs (GNS-1481, GNS-1486). The improved, potent mutant-EGFR selective agents that we describe here show two important advantages over the currently approved EGFR TKIs, including osimertinib: (1) less WT EGFR inhibition and, therefore, risk of toxicity while exhibiting substantial anti-tumor efficacy and (2) improved potency against CNS metastasis. Given these distinct attributes, these new EGFR TKIs complement the currently approved EGFR TKIs and are now under clinical development; indeed, clinical trials testing these new agents in EGFR-mutant (including $EGFR^{T790M}$) LA patients with active CNS and extracranial metastatic disease will be initiated soon. While only these clinical trials can establish whether the greater selectivity for mutant EGFR versus WT EGFR and the increased potency against CNS disease that we observed in the preclinical systems will yield improved outcomes and safety in patients, these promising new agents have the potential to exhibit efficacy in patients with both extracranial and intracranial EGFR-mutant LA (including $EGFR^{T790M}$-positive disease), with less clinical toxicity, to thereby potentially improve not only the quantity but also quality of life for patients. Our study highlights the utility of identifying highly potent and oncoprotein-selective targeted agents that show substantial activity against CNS metastasis early in the drug discovery and development process to reduce both clinical toxicity and the high burden and related mortality of CNS metastasis, as well as extracranial disease, in patients.

Supplementary Material

Refer to Web version on PubMed Central for supplementary material.

Acknowledgments

Financial support. This study was supported by the Basic Science Research Program through the National Research Foundation of Korea (NRF, grant 2013R1A1A2005112 to J.K. Rho and grant 2014R1A2A2A01003438 to J.C. Lee) and a grant of the Korea Health Technology R&D Project through the Korea Health Industry Development Institute (KHIDI), funded by the Ministry of Health & Welfare, Republic of Korea (grant HI15C0516). T.G. Bivona acknowledges support from NIH (NIH Director's New Innovator Award, grant DP2 CA174497 and grant R01 CA169338).

References

1. Cancer Genome Atlas Research N. Comprehensive molecular profiling of lung adenocarcinoma. Nature. 2014; 511(7511):543–550. [PubMed: 25079552]
2. Swanton C, Govindan R. Clinical Implications of Genomic Discoveries in Lung Cancer. The New England journal of medicine. 2016; 374(19):1864–1873. [PubMed: 27168435]

3. Lynch TJ, et al. Activating mutations in the epidermal growth factor receptor underlying responsiveness of non-small-cell lung cancer to gefitinib. The New England journal of medicine. 2004; 350(21):2129–2139. [PubMed: 15118073]
4. Pao W, et al. EGF receptor gene mutations are common in lung cancers from “never smokers” and are associated with sensitivity of tumors to gefitinib and erlotinib. Proceedings of the National Academy of Sciences of the United States of America. 2004; 101(36):13306–13311. [PubMed: 15329413]
5. Paez JG, et al. EGFR mutations in lung cancer: correlation with clinical response to gefitinib therapy. Science. 2004; 304(5676):1497–1500. [PubMed: 15118125]
6. Rosell R, et al. Screening for epidermal growth factor receptor mutations in lung cancer. The New England journal of medicine. 2009; 361(10):958–967. [PubMed: 19692684]
7. Mok TS, et al. Gefitinib or carboplatin-paclitaxel in pulmonary adenocarcinoma. The New England journal of medicine. 2009; 361(10):947–957. [PubMed: 19692680]
8. Soda M, et al. Identification of the transforming EML4-ALK fusion gene in non-small-cell lung cancer. Nature. 2007; 448(7153):561–566. [PubMed: 17625570]
9. Shaw AT, et al. Crizotinib versus chemotherapy in advanced ALK-positive lung cancer. The New England journal of medicine. 2013; 368(25):2385–2394. [PubMed: 23724913]
10. Rosell R, Bivona TG, Karachaliou N. Genetics and biomarkers in personalisation of lung cancer treatment. Lancet. 2013; 382(9893):720–731. [PubMed: 23972815]
11. Bivona TG, Doebele RC. A framework for understanding and targeting residual disease in oncogene-driven solid cancers. Nat Med. 2016; 22(5):472–478. [PubMed: 27149220]
12. Politi K, Ayeni D, Lynch T. The Next Wave of EGFR Tyrosine Kinase Inhibitors Enter the Clinic. Cancer Cell. 2015; 27(6):751–753. [PubMed: 26058074]
13. Garraway LA, Janne PA. Circumventing cancer drug resistance in the era of personalized medicine. Cancer discovery. 2012; 2(3):214–226. [PubMed: 22585993]
14. Sawyers CL. The 2011 Gordon Wilson Lecture: overcoming resistance to targeted cancer drugs. Transactions of the American Clinical and Climatological Association. 2012; 123:114–123. discussion 123–115. [PubMed: 23303979]
15. Pazarentzos E, Bivona TG. Adaptive stress signaling in targeted cancer therapy resistance. Oncogene. 2015
16. Bivona TG, et al. FAS and NF-kappaB signalling modulate dependence of lung cancers on mutant EGFR. Nature. 2011; 471(7339):523–526. [PubMed: 21430781]
17. Crystal AS, et al. Patient-derived models of acquired resistance can identify effective drug combinations for cancer. Science. 2014; 346(6216):1480–1486. [PubMed: 25394791]
18. Hrustanovic G, et al. RAS-MAPK dependence underlies a rational polytherapy strategy in EML4-ALK-positive lung cancer. Nat Med. 2015; 21(9):1038–1047. [PubMed: 26301689]
19. Owonikoko TK, et al. Current approaches to the treatment of metastatic brain tumours. Nat Rev Clin Oncol. 2014; 11(4):203–222. [PubMed: 24569448]
20. Ali A, Goffin JR, Arnold A, Ellis PM. Survival of patients with non-small-cell lung cancer after a diagnosis of brain metastases. Curr Oncol. 2013; 20(4):e300–306. [PubMed: 23904768]
21. Camidge DR, Pao W, Sequist LV. Acquired resistance to TKIs in solid tumours: learning from lung cancer. Nat Rev Clin Oncol. 2014; 11(8):473–481. [PubMed: 24981256]
22. Yu HA, et al. Analysis of tumor specimens at the time of acquired resistance to EGFR-TKI therapy in 155 patients with EGFR-mutant lung cancers. Clinical cancer research : an official journal of the American Association for Cancer Research. 2013; 19(8):2240–2247. [PubMed: 23470965]
23. Walter AO, et al. Discovery of a mutant-selective covalent inhibitor of EGFR that overcomes T790M-mediated resistance in NSCLC. Cancer discovery. 2013; 3(12):1404–1415. [PubMed: 24065731]
24. Cross DA, et al. AZD9291, an irreversible EGFR TKI, overcomes T790M-mediated resistance to EGFR inhibitors in lung cancer. Cancer discovery. 2014; 4(9):1046–1061. [PubMed: 24893891]
25. Sequist LV, et al. Rociletinib in EGFR-mutated non-small-cell lung cancer. The New England journal of medicine. 2015; 372(18):1700–1709. [PubMed: 25923550]

26. Janne PA, et al. AZD9291 in EGFR inhibitor-resistant non-small-cell lung cancer. The New England journal of medicine. 2015; 372(18):1689–1699. [PubMed: 25923549]
27. Thress KS, et al. Acquired EGFR C797S mutation mediates resistance to AZD9291 in non-small cell lung cancer harboring EGFR T790M. Nat Med. 2015
28. Piotrowska Z, et al. Heterogeneity Underlies the Emergence of EGFR T790 Wild-Type Clones Following Treatment of T790M-Positive Cancers with a Third Generation EGFR Inhibitor. Cancer discovery. 2015
29. Lin L, Bivona TG. Mechanisms of Resistance to Epidermal Growth Factor Receptor Inhibitors and Novel Therapeutic Strategies to Overcome Resistance in NSCLC Patients. Chemother Res Pract. 2012; 2012:817297. [PubMed: 22970367]
30. Ballard P, et al. Preclinical Comparison of Osimertinib with Other EGFR-TKIs in EGFR-Mutant NSCLC Brain Metastases Models, and Early Evidence of Clinical Brain Metastases Activity. Clinical cancer research : an official journal of the American Association for Cancer Research. 2016
31. Ricciuti B, et al. Osimertinib (AZD9291) and CNS Response in Two Radiotherapy-Naive Patients with EGFR-Mutant and T790M-Positive Advanced Non-Small Cell Lung Cancer. Clinical drug investigation. 2016
32. Yu HA, et al. Acquired Resistance of EGFR-Mutant Lung Cancer to a T790M-Specific EGFR Inhibitor: Emergence of a Third Mutation (C797S) in the EGFR Tyrosine Kinase Domain. JAMA oncology. 2015; 1(7):982–984. [PubMed: 26181354]
33. Rho JK, et al. The role of MET activation in determining the sensitivity to epidermal growth factor receptor tyrosine kinase inhibitors. Mol Cancer Res. 2009; 7(10):1736–1743. [PubMed: 19808904]
34. Carlomagno F, et al. Disease associated mutations at valine 804 in the RET receptor tyrosine kinase confer resistance to selective kinase inhibitors. Oncogene. 2004; 23(36):6056–6063. [PubMed: 15184865]
35. Takeuchi K, et al. RET, ROS1 and ALK fusions in lung cancer. Nat Med. 2012; 18(3):378–381. [PubMed: 22327623]
36. Marusiak AA, et al. Mixed lineage kinases activate MEK independently of RAF to mediate resistance to RAF inhibitors. Nat Commun. 2014; 5:3901. [PubMed: 24849047]
37. Tricker EM, et al. Combined EGFR/MEK Inhibition Prevents the Emergence of Resistance in EGFR-Mutant Lung Cancer. Cancer discovery. 2015; 5(9):960–971. [PubMed: 26036643]
38. Rho JK, et al. Combined treatment with silibinin and epidermal growth factor receptor tyrosine kinase inhibitors overcomes drug resistance caused by T790M mutation. Mol Cancer Ther. 2010; 9(12):3233–3243. [PubMed: 21159609]
39. Zhang Z, et al. Activation of the AXL kinase causes resistance to EGFR-targeted therapy in lung cancer. Nat Genet. 2012; 44(8):852–860. [PubMed: 22751098]
40. Rho JK, et al. MET and AXL inhibitor NPS-1034 exerts efficacy against lung cancer cells resistant to EGFR kinase inhibitors because of MET or AXL activation. Cancer Res. 2014; 74(1):253–262. [PubMed: 24165158]

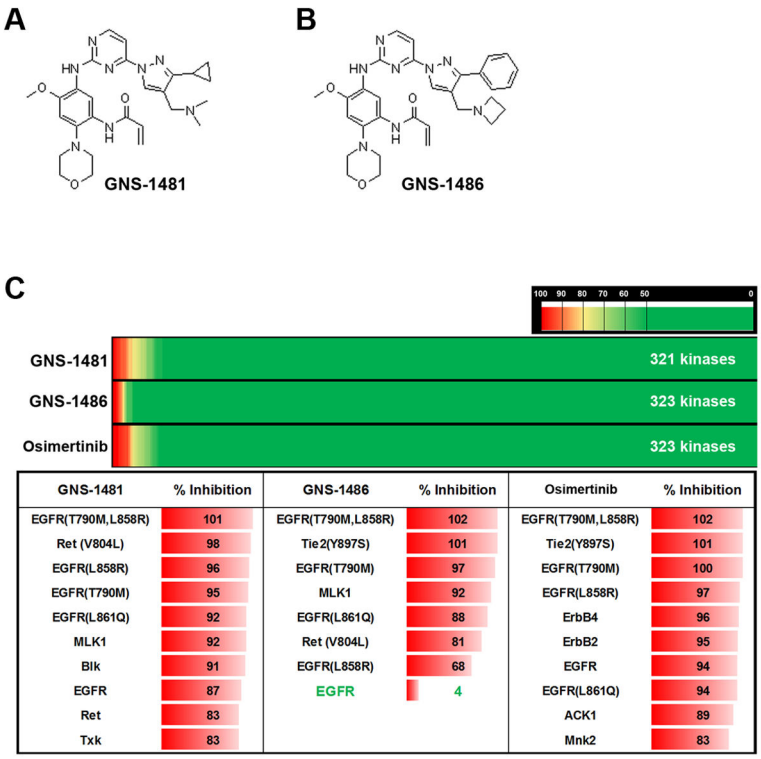

Figure 1. Characterization of the novel mutant-selective EGFR kinase inhibitors GNS-1481 and GNS-1486

(A) Chemical structure of GNS-1481. (B) Chemical structure of GNS-1486. (C) Selectivity and target profile of 1 μM GNS-1481 and GNS-1486 (and AZD9291 for comparison) against ~320 kinases in a multi-kinase inhibition assay *in vitro*. Shown are kinases whose activity is inhibited by >80% at the dose tested, with red indicating 100% inhibition, yellow indicating 80% inhibition, and green < 50% inhibition of each target profiled.

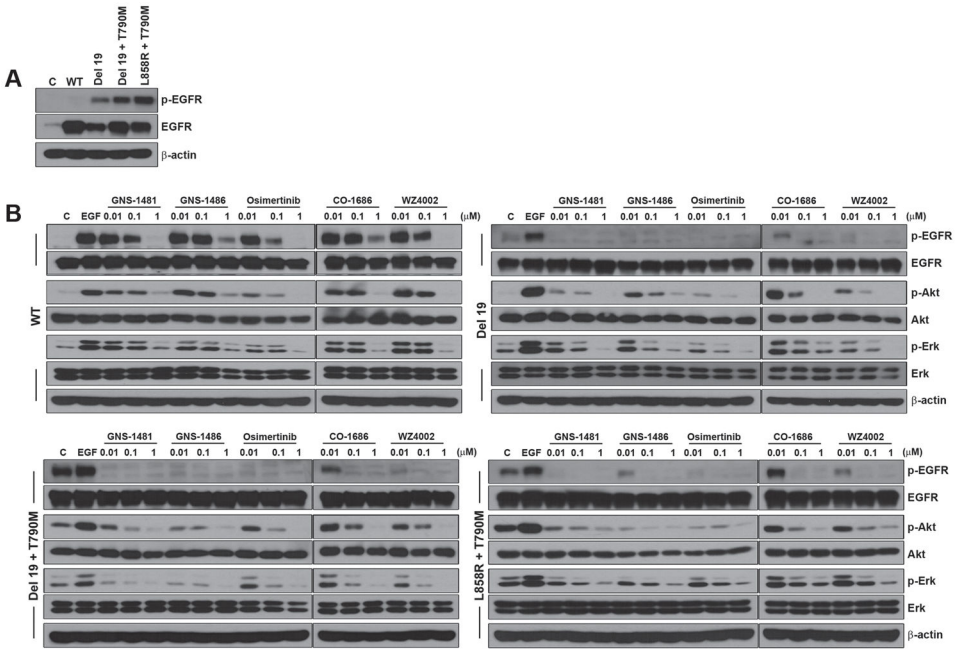

Figure 2. Preclinical efficacy of the novel mutant-selective EGFR kinase inhibitors GNS-1481 and GNS-1486 *in vitro*

(A–B) Effects of treatment with the indicated EGFR kinase inhibitors on the indicated signaling components in the indicated NIH-3T3 cell lines engineered to stably express either WT EGFR or each form of mutant EGFR shown. Effects of treatment with the indicated EGFR kinase inhibitors (for 5 hours) on the indicated signaling components are shown. Results represent at least 3 independent experiments.

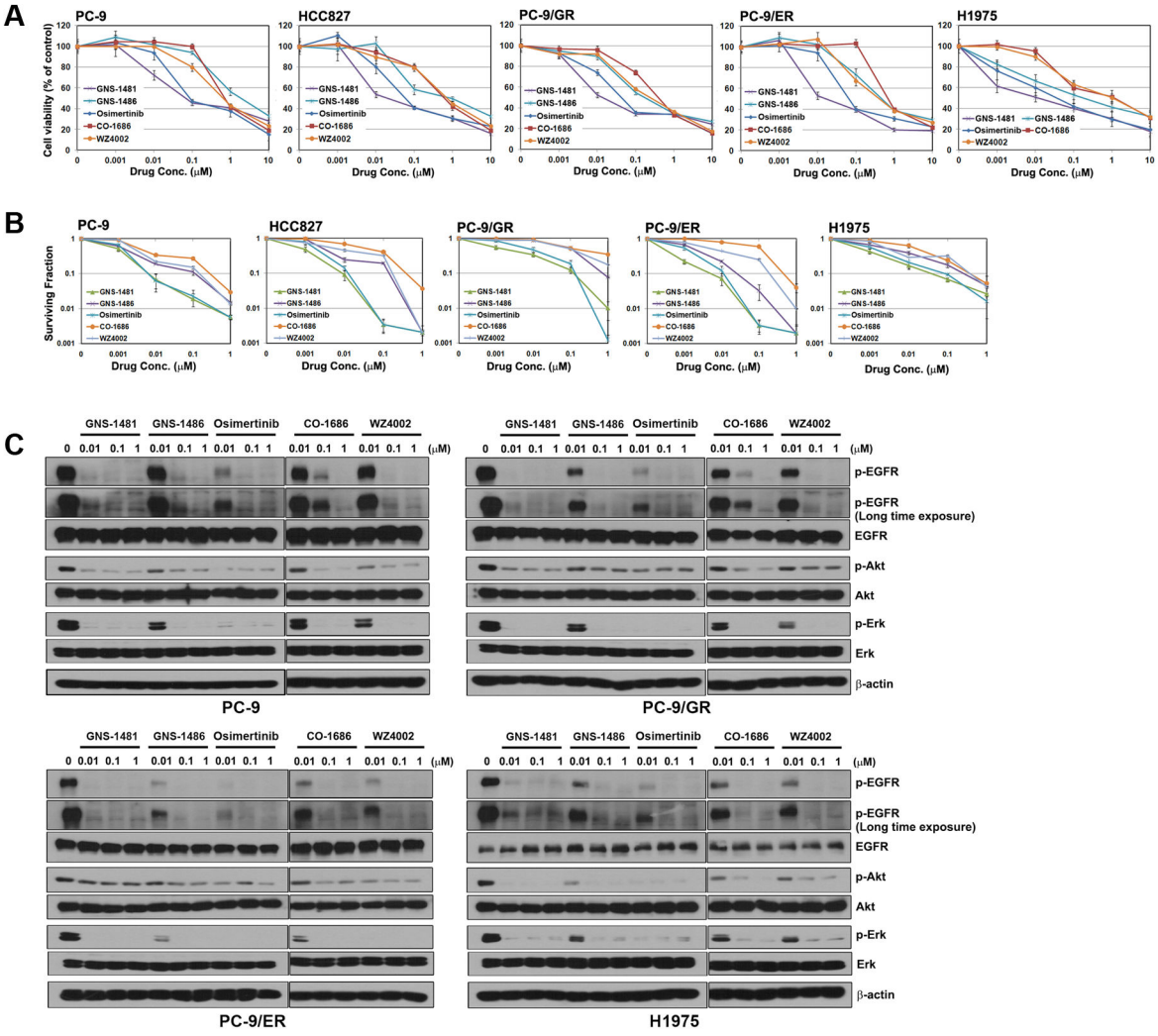

Figure 3. Preclinical efficacy of the novel mutant-selective EGFR kinase inhibitors GNS-1481 and GNS-1486 *in vitro* in lung cancer models

(A–B) Effects of treatment with the indicated EGFR kinase inhibitors on cell viability in the indicated human lung adenocarcinoma cell lines with endogenous mutant EGFR (n=3, ±SEM). The sensitivity to EGFR inhibitor treatment was determined by MTT assay (A) and colony formation assay (B). (C) Effects of treatment with the indicated EGFR kinase inhibitors (for 5 hours) on the indicated signaling components in the cell lines in (A–B). Results represent at least 3 independent experiments.

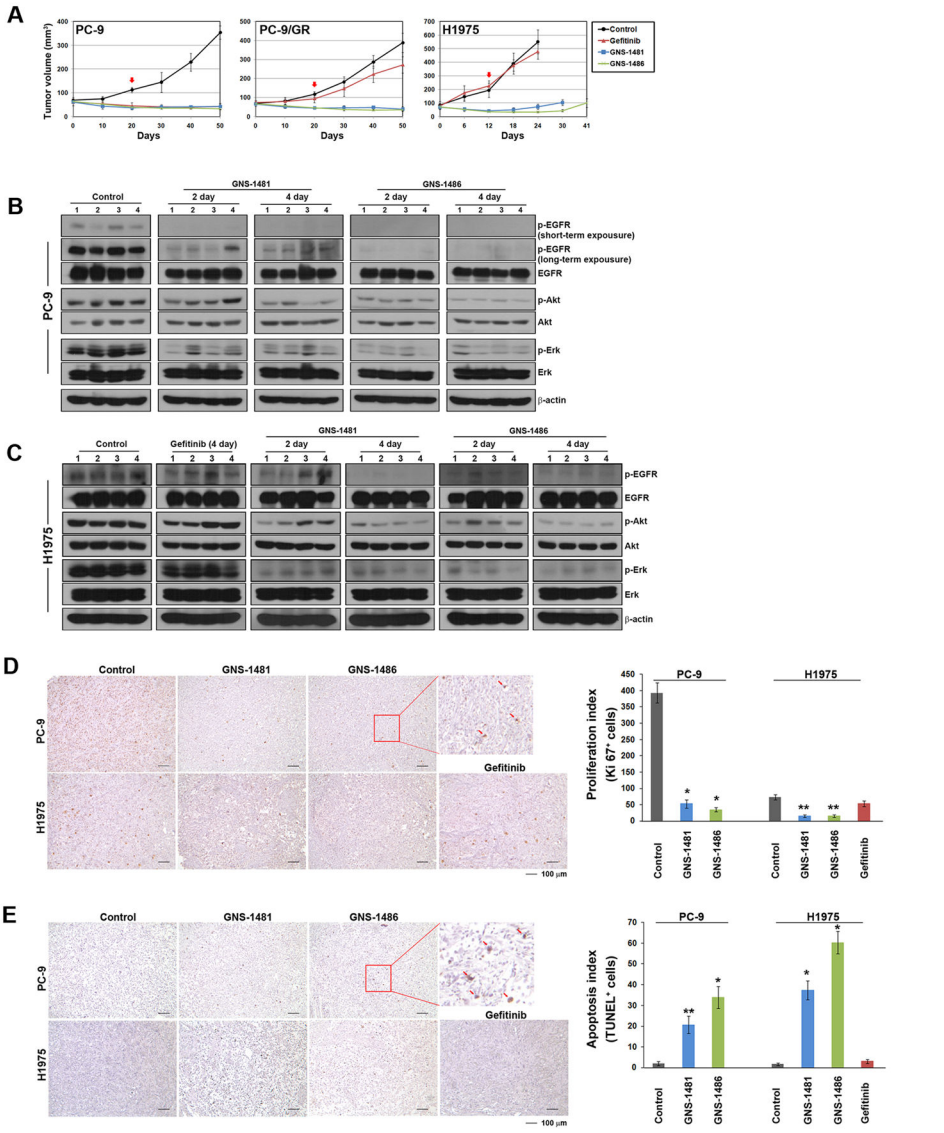

Figure 4. Preclinical efficacy of the novel mutant-selective EGFR kinase inhibitors GNS-1481 and GNS-1486 *in vivo*

(A) *In vivo* anti-tumor efficacy of the indicated EGFR inhibitors in the subcutaneous tumor xenografts in mice (n=5 per treatment cohort for each xenograft model). Mice were treated orally with vehicle or 30 mg/kg/day GNS-1481 or GNS-1486 or 100 mg/kg/day of gefitinib daily (5 consecutive days/week). Results are shown as tumor volume measurements over the time course of treatment with vehicle control or each EGFR inhibitor and presented as ± SEM. Each treatment was initiated at Day 0, and the red arrow indicates cessation of each therapy, with continued measurement of tumor volumes to the endpoint. (B–C) Immunoblot analysis measuring each indicated pharmacodynamic biomarker in representative control-treated or EGFR inhibitor-treated tumors harvested from tumor-bearing mice at the indicated time points following the initiation of therapy. (B) shows the analysis of PC-9 tumors and (C) shows the analysis of H1975 tumors. Results represent at least 3 independent experiments. (D–E) Immunohistochemistry analysis measuring each indicated

pharmacodynamic biomarker (D, shows Ki-67 and E, shows TUNEL staining) in representative control-treated or EGFR inhibitor-treated tumors harvested from tumor-bearing mice at 4 days following the initiation of therapy. Inset on the right shows quantification of the Ki-67 and TUNEL staining in (D–E) under each condition. *P<0.01, and **P<0.001 for GNS-1481 or GNS-1486 versus control (vehicle-treated) tumors.

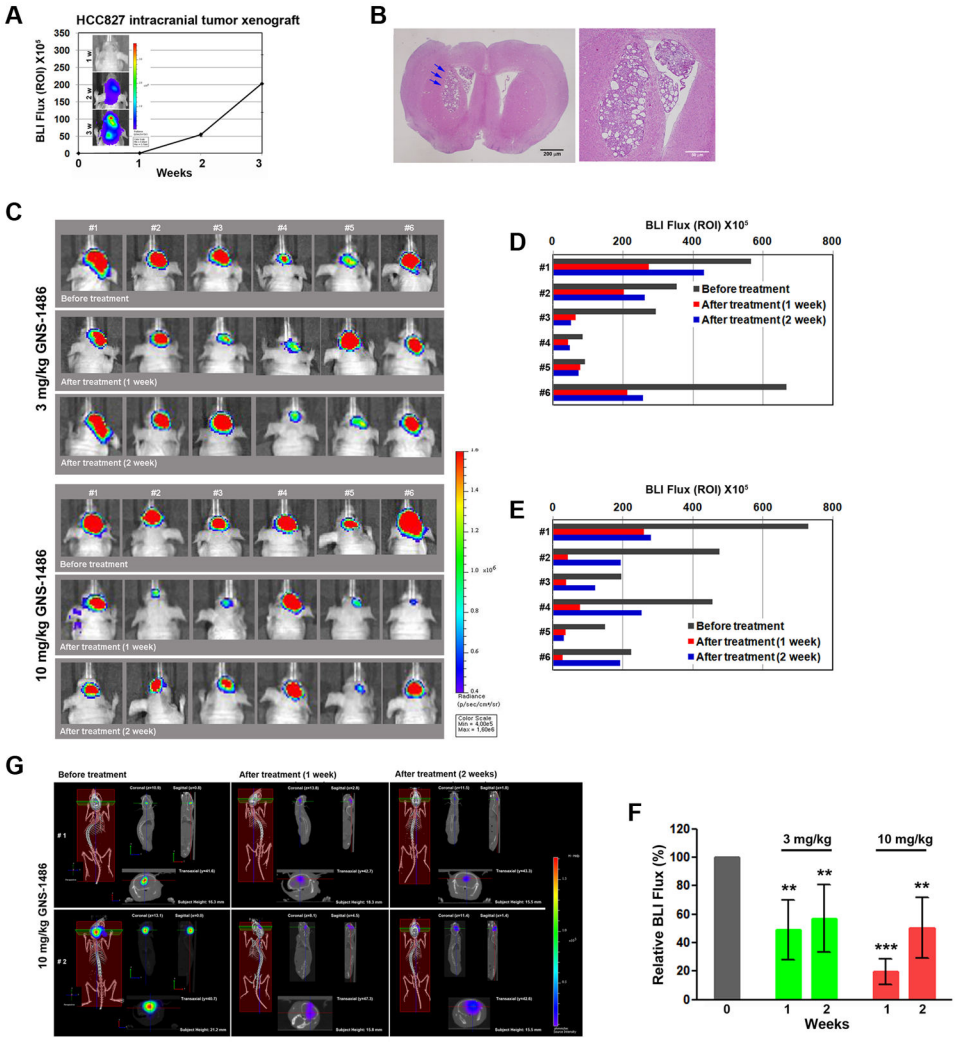

Figure 5. Intracranial anti-tumor efficacy of the novel mutant-selective EGFR kinase inhibitor GNS-1486 *in vivo*

(A) Establishment of the EGFR-mutant lung adenocarcinoma intracranial model using HCC827 cells stably expressing the Luciferase reporter (HCC827-Luc). Bioluminescence imaging (BLI) was used to detect and monitor intracranial tumor growth *in vivo*. Shown is a representative mouse with intracranial tumor growth within 3 weeks following intracranial implantation. (B) Histologic analysis of HCC827-Luc tumor in a representative mouse following intracranial implantation. Hematoxylin and eosin (H&E) staining of tumor sections obtained following intracranial tumor harvest from an individual mouse shows lung adenocarcinoma formation in the brain. Arrows indicate areas of tumor in the brain parenchyma. (C–G) Bioluminescence imaging (BLI) micro-CT images, and quantification analysis of intracranial HCC827-Luc tumor growth before and during oral treatment with GNS-1486 (5 consecutive days/week, n=6 animals) at the indicated time points and drug doses. Red pseudo-coloring indicates increased tumor growth and green-blue pseudo-coloring indicates decreased tumor growth by bioluminescence quantification in (C,G). (D,E,F) Quantification of the bioluminescence photon flux in the mice with intracranial

HCC827-Luc tumors treated over the indicated time points. *P<0.01 and **P<0.001 **P<0.0001 for drug versus control (vehicle-treated) tumors. For all treatment studies, baseline imaging and subsequent therapy was initiated 14 days following intracranial tumor cell implantation.

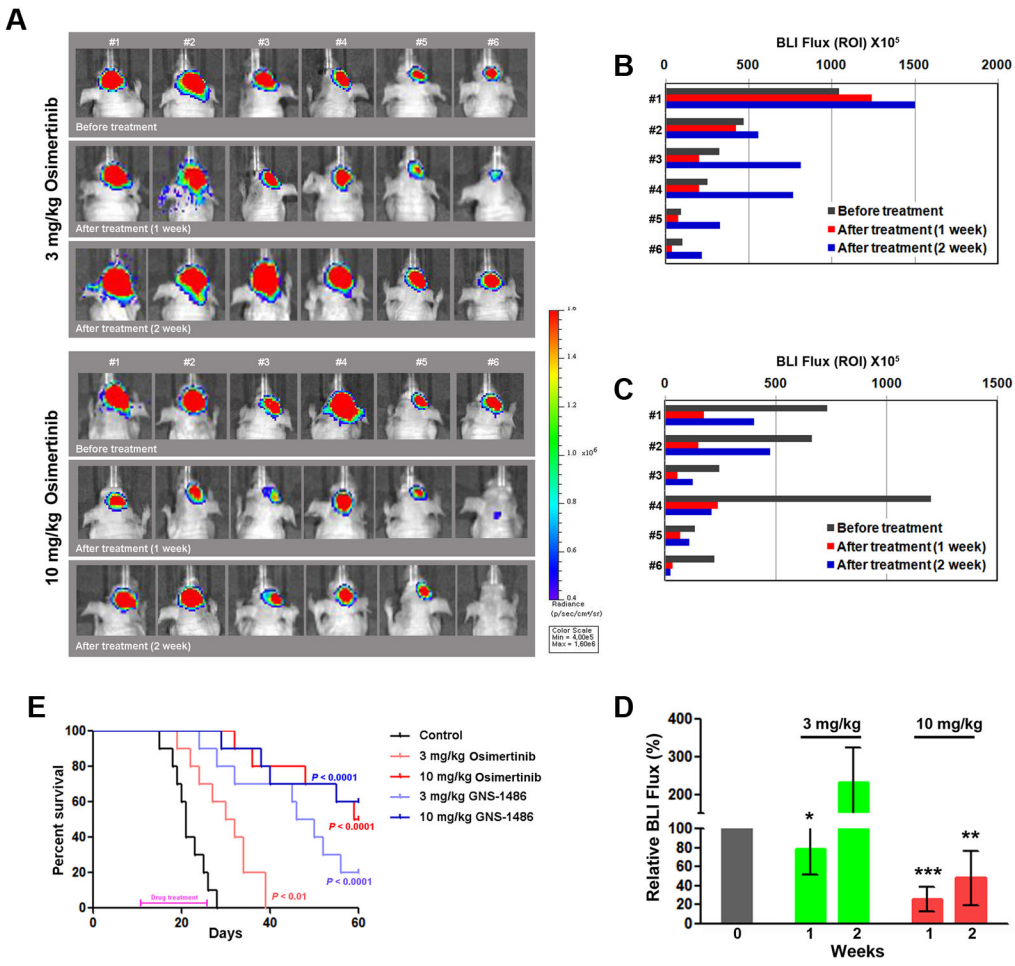

Figure 6. Intracranial anti-tumor efficacy of GNS-1486 and osimertinib *in vivo*

(A–D) Bioluminescence imaging (BLI) micro-CT images, and quantification analysis of intracranial HCC827-Luc tumor growth before and during oral treatment with osimertinib (5 consecutive days/week, n=6 animals) at the indicated time points and drug doses. Red pseudo-coloring indicates increased tumor growth and green-blue pseudo-coloring indicates decreased tumor growth by bioluminescence quantification in (A). (B,C,D) Quantification of the bioluminescence photon flux in the mice with intracranial HCC827-Luc tumors treated over the indicated time points. *P<0.01 and **P<0.001 **P<0.0001 for drug versus control (vehicle-treated) tumors. (E) Kaplan-Meier survival curves of HCC827-Luc cell line in mice treated the indicated oral doses of either GNS-1486 or AZD9291 daily for 2 weeks, indicated by the purple line on the x-axis (n=7 animals per cohort, *P* values shown compared to control treatment). For all treatment studies, baseline imaging and subsequent therapy was initiated 14 days following intracranial tumor cell implantation.

Table 1

Multi-kinase inhibition profiles for GNS-1481 and GNS-1486, and the other indicated EGFR kinase inhibitors

Shown is the half-maximal inhibitory concentration (IC_{50}) in nanomolar (nM) of each drug against the kinase activity of each indicated protein. The bottom row indicates the mutant-selective index (increased proportional to the degree of mutant-selective activity, ratio calculated as the IC_{50} WT EGFR/ L858R-T790M double mutant).

	Kinase	GNS-1481	GNS-1486	Osimertinib	CO-1686	Afatinib	Erlotinib
EGFR	Wild type	26.5	121.6	16.7	928.2	0.2	0.6
	Del 19 (E746-A750)	6.6	20.5	8.6	216.5	0.2	0.8
	L858R	25.8	103.6	12.2	742.9	0.3	0.9
	Double Mutant (L858R-T790M)	6.2	8.3	4.5	45.7	18.6	549.3
	T790M	3.4	4.2	2.2	20.5	1.6	395.2
	Double Mutant (Del 19-T790M)	4.2	4.3	3.3	44.1	7.0	715.6
	Wild type/Double Mutant (L858R-T790M)	4.3	14.7	3.7	20.3	0.01	< 0.01